Experiments in Fluids 16, 171–180 (1994)

Experiments in Fluids

Measurements of the vaporization dynamics in the development zone of a burning spray by planar laser induced fluorescence and Raman scattering

R. Bazile, D. Stepowski

URA CNRS 230 CORIA, University of Rouen, F-76134 Mont Saint Aignan, France

Received: 23 March 1993 / Accepted: 25 June 1993

Abstract. A linear measurement technique based on simultaneous planar imaging of laser induced dye fluorescence and Raman scattering in the liquid phase is reported. Calibrations in a stream of monosized droplets doped with weak concentrations of rhodamin show that the intensities on the droplet images are proportional to the actual droplet volume for Raman scattering and to the initial volume of the droplet for fluorescence, as the mass of dissolved dye does not vaporize. Thus, the mass fraction of liquid fuel that has vaporized before the probing event can be derived from these simultaneous measurements. Experiments are performed in the early development of a burning spray to derive cumulative information on the vaporization dynamics in terms of mass fraction or evaporation constant. Size distribution from conjoined phase-Doppler measurements are also used to derive the rate of droplet consumption along the axis of the burning spray.

1 Introduction

Knowledge of the state and dynamics of fuel vaporization in the development zone of a burning spray is useful for investigating the different combustion regimes and structures that may be involved in flame stabilization. Owing to the strong density differences between condensed and vapor phase, and to the limited dynamic range of the detectors, the laser induced emissions from the vaporized phase are very difficult to extract from those induced in the liquid.

Laser diagnostics based on elastic interactions are practically unapplicable as the scattered intensities, which are emitted basically at the laser wavelength, are at least six orders of magnitude lower for the gas phase (Rayleigh range) than they are for the droplets (upper Mie range). However, some improvements can be expected (Miles et al. 1990) by using the Doppler broadening due to thermal agitation in the vapor to reject the monochromatic radiation scattered by the droplets, provided that narrowband spectral filtering can be achieved.

Correspondence to: D. Stepowski

The laser techniques based on Raman and fluorescence interactions provide emissions at specific wavelengths whose frequency shifts are practically insensitive to the phase in which the probed molecules are found. Thus, these spectroscopic techniques can reject the elastic light scattering by the droplets but they cannot discriminate between liquid and vaporized phase contributions of a given molecule. Very promising results have been obtained by the exciplex fluorescence technique (Melton and Verdieck 1985) in which a laser assisted reaction between organic additives occurs predominantly in condensed phase to form an excited-state complex—called exciplex—whose fluorescence is well red shifted with respect to that of the excited monomer in the vapor phase. Unfortunately this technique is very difficult to apply in a flame as the excited monomer is strongly quenched by oxygen.

In the exciplex fluorescence method the liquid additives that have been doped into the fuel are assumed to be co-evaporative with it. Alternatively, the present paper reports on development and application of a different method in which the liquid fuel (methanol) has been doped with a very low concentration of an organic dye (rhodamin 6G) which does not vaporize. The local concentration of dissolved dye is probed by laser induced fluorescence while the liquid fuel concentration is simultaneously available from the Raman scattering induced by the same laser pulse. Then the mass fraction of liquid fuel that have been vaporized can be derived from these simultaneous measurements. This method provides the cumulative mass of vaporized fuel over the liquid course up to the measurement rather than the local mass of fuel vapor, but—perhaps more interestingly—it can provide useful information on the vaporization dynamics. The field of application of this technique is bound by the dynamic limits of the detector but, now, the measurement is insensitive to the thermochemical environment (collisional quenching), as both the dye and the fuel liquid molecules are laser probed in the same condensed phase.

2 Spontaneous Raman scattering from methanol

As methanol is linearly excited by a UV laser ($\lambda_0 = 284$ nm, $I_0 \approx 1$ MW/cm^2) the molecules scatter Raman shifted radiations ($\lambda_1 = 308.9$ nm, $\lambda_2 = 309.9$ nm, $\lambda_3 = 292.5$ nm) which are mainly dues to the stretching vibration modes of CH ($\Delta\nu_1 = 2837$ cm^{-1}, $\Delta\nu_2 = 2942$ cm^{-1}) and CO ($\Delta\nu_3 = 1029$ cm^{-1}) (Herzberg 1945). Such UV excitation is efficient, first because the Raman scattering cross section is proportional to λ^{-4}. Second, the range of Raman wavelength shifts makes it possible to reject both the elastic radiation from Mie scattering and the yellow dye fluorescence that is involved later (Sect. 3), using a pass-band filter. Though this Raman signal is four times lower when laser excitation and detection optics are cross polarized, the rejection of Mie scattering is further improved by this perpendicular polarization arrangement. Under linear excitation and with caution that no absorption nor optical breakdown occur, the Raman scattering intensity is proportional (through the bandwidth factor) to the number of molecules in the probed volume.

Experiments (Johnston 1981) have shown that the Raman spectra in liquid and vapor phases are nearly identical except for a pure rotational structure that would be extremely difficult to discrimate against the very close laser frequency. Thus, broadband detection of vibrational Raman scattering, such as performed in the present work, cannot extract the vaporized methanol contribution. Because of the much greater molecular density in the liquid phase compared to the vapor phase, the Raman scattering intensity from the vaporized methanol is always below the detection threshold, as the detector gain is restricted in order to avoid saturation by the liquid phase signal. Thus, over the linear dynamic range, the detected signal is proportional to the mass of liquid methanol in the probed volume as the bandwidth factor is constant in the condensed phase. Furthermore, when a single droplet is linearly excited by homogeneous radiation, the total number of photo-counts on its space resolved Raman image is proportional to the droplet volume (i.e. $\sim d^3$) in so far as this count number falls within the linearity range of the imaging system. Validation and calibration experiments for these linear dependencies are reported in Sect. 4.

Figure 1 shows an example of planar Raman imaging of liquid methanol just above a coaxial airblast injector (details are provided in Sect. 4). The height of the laser sheet has been limited to 20 mm with a diaphragm to ensure a constant laser irradiance (within 10%) over the incident field. Both laser and Raman radiation are not absorbed by methanol, but, as can be expected in view of the instantaneous liquid structure, the incident laser sheet (300 μm thick) is likely to be distorted and thickened when propagating through the sharp index gradients. A non-linear color scaling has been used to visualize the strong gradients but the marked signal levels which are proportional to the energy onto the camera, are a direct measure of the local mass fraction of liquid fuel in the laser field. However, unavoidable uncertainties on the spatial resolution remain, as both laser and Raman radiations may be refracted in the high gradient zones.

It is worth noting that the contribution of the small droplets that are detected (Fig. 1a) on the single shot images is no longer visible on the ensemble average picture (Fig. 1b) that has been post processed, although it could be made visible in the outer zones of the jet by picturing the restored image levels with a non-linear scale. This dynamic limitation which can never be overcome when either space or time integrations are basically involved in a diagnostic, underscores the requirement of statistical analyses based on instantaneous space resolved measurements. The minimum droplet diameter that can be derived from the signal level on its Raman image is about 50 μm which corresponds to two resolved elements on the laser plane.

3 Dye fluorescence

When a very small amount of dye (rhodamin 6G) is dissolved in liquid methanol ($C_0 \approx 0.02$ ppm) the UV laser pulse induces a yellow fluorescence emission over a broad spectral range [525–610 nm] which is determined by the spectroscopic structure of the dissolved dye molecule. The UV Raman scattering from methanol which is simultaneously induced—without any noticeable modification due to the presence of the dye—can be easily discriminated with a pass-band filter (see Fig. 2). Then, as the dye population is so low that laser absorption and fluorescence trapping are negligible, the fluorescence intensity is proportional to the mass of dissolved dye in the probed volume since the fluorescence yield is fixed by the constant rate of quenching collisions with methanol molecules. However, measurement and calibration (see section 4) of the fluorescence signal must be performed in a flowing liquid to avoid cumulative dye photolysis by the UV radiation.

Rhodamin 6G is an ionic molecule with a very low vapor pressure whose vaporization is negligible compared to that of methanol. Experiments have ascertained that no fluorescence is induced in the condensate from fast distillation of a concentrated dye solution. Thus, the laser induced fluorescence intensity from a spray is not sensitive to vaporization compared to the simultaneous Raman scattering intensity which decreases with the mass fraction of liquid methanol. However, when the dye concentration approaches a critical value, C^*, the rate of quenching collisions between dye molecules must be accounted for

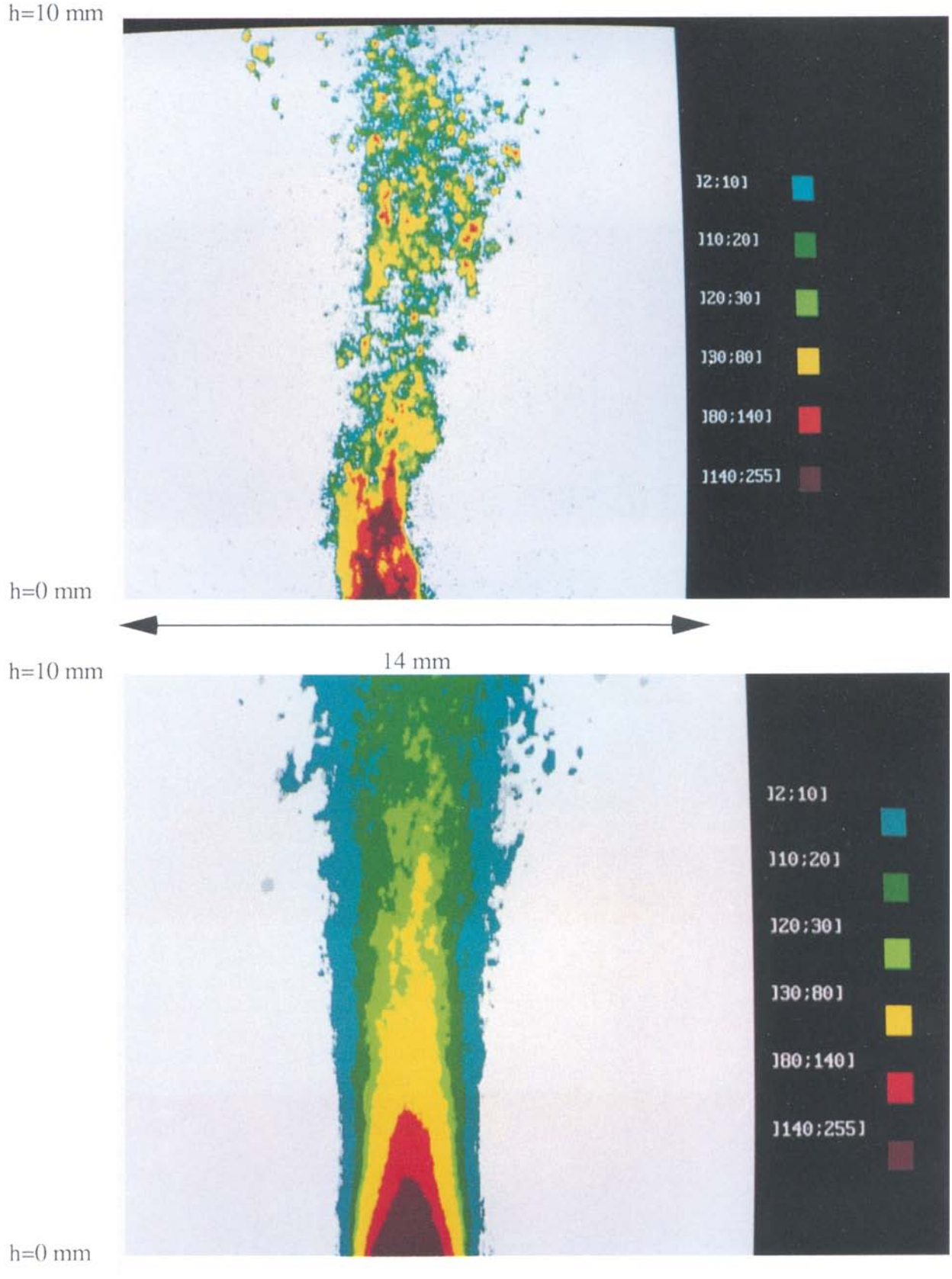

Fig. 1a, b. Planar Raman imaging of liquid methanol just above the coaxial air/blast injector. The marked signal levels are proportional to the mass fraction of liquid fuel in the laser field. **a** Single shot image; **b** Ensemble average picture over 200 laser shots

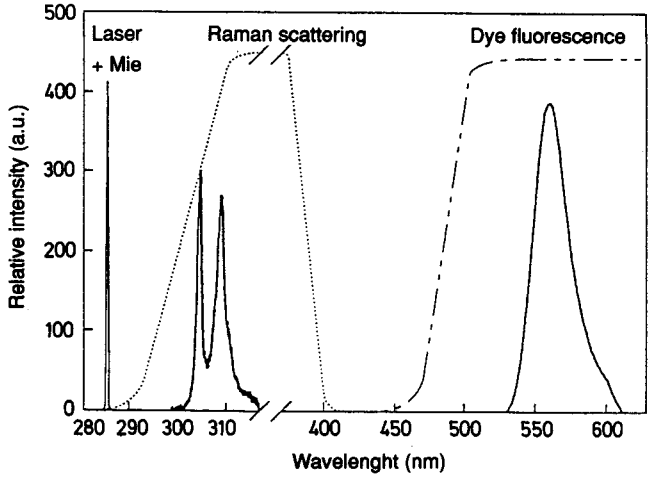

Fig. 2. Spectral locations of methanol Raman scattering and dye laser induced fluorescence as selected by pass-band filters

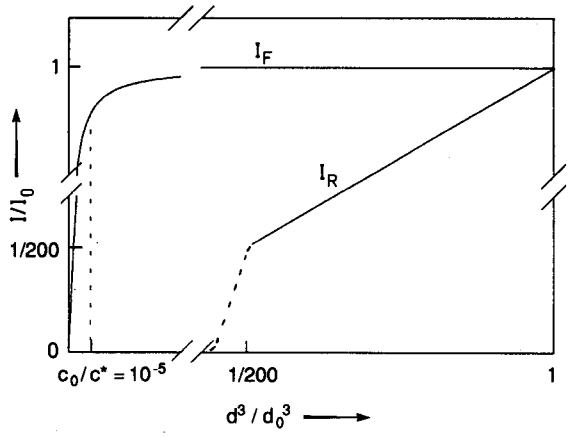

Fig. 3. Schematized evolution of the Raman and dye fluorescence intensities emitted by a single droplet as a function of volume reduction

(Bruhat 1992) and the fluorescence yield ρ drops according to the Perrin's law:

$$\rho = \rho_0 \, e^{\frac{-C}{C^*}} \tag{1}$$

Thus, as a doped droplet with initial diameter d_0 vaporizes, the fluorescence intensity from the dissolved dye in that droplet is:

$$I_f \equiv C \, d^3 \, \rho \equiv C_0 \, d_0^3 \, \rho_0 \, \exp\left(-\frac{C_0 d_0^3}{C^* d^3}\right) \tag{2}$$

With $C_0/C^* \approx 10^{-5}$, the fluorescence intensity is constant within 1%, provided that $d_0^3/d^3 < 10^3$, which is higher than the dynamic range of the imaging system (~ 200). Thus, in so far as the Raman signal intensity from a single droplet is proportional to the droplet volume ($\approx d^3$), the intensity of the dye fluorescence signal is proportional to the initial volume of that droplet ($\approx d_0^3$) before any vaporization has occurred (see Fig. 3). Hence, provided that accurate signal calibrations have been made, the difference between fluorescence and Raman intensities in a given probed volume can provide the mass of methanol that has been vaporized. However, part of the liquid, and the fraction of vaporized fuel from that part, are not accounted for as the fluorescence yield drops to zero when $d^3/d_0^3 < 10^{-5}$.

4 Calibrations

The calibration experiments have been performed in a stream of monosized droplets from a vibrating needle fed with diluted solutions of dye in methanol. Drop size [120–450 μm] was monitored by adjusting the needle frequency f and the liquid flow rate Q_v according to $d_0^3 = 6Q_v/\pi f$. The droplet size stability was controlled by stroboscopic measurement, and the mean droplet diameter was accurately determined ($\pm 4\%$) by weighting technique.

Figure 4a shows examples of dye fluorescence and Raman scattering images of the monosized droplets as a single UV laser pulse ($\lambda = 284$ nm, $\Delta t = 10$ ns) is focused in the stream in a light sheet thicker (1 mm) than the droplet size. Under these conditions ($I_0 \approx 0.3$ MW·cm^{-2}, $d_0/\lambda > 400$, $C_{dye} < 4$ ppm), no lasing nor stimulated Raman radiations are induced by morphology-dependent resonances (Serpenguzel et al.) as the threshold of such nonlinear effects is not reached. As plotted in Fig. 4b, the integrated intensity of both the dye fluorescence and the Raman scattering on a single droplet image is proportional to its volume ($\approx d_0^3$). Furthermore, the fluorescence signal from a 310 μm droplet with a given dye concentration was the same as that from a 245 μm droplet with twice that dye concentration. Thus, as the fluorescence signal intensity is proportional to the mass of dissolved dye in a droplet irrespective of drop size, the Raman and fluorescence signal levels can be preliminary equalized in a non vaporizing stream by adjusting the dye concentration in the liquid reservoir. Then, any intensity difference between fluorescence and Raman signal within the linear range of detection can be imputed to vaporization effects. However, when the comparison is made in terms of size reduction for space resolved droplets, one must make sure that the probed droplets are completely inside the laser sheet. A criterion for this is provided by the ratio:

$$\alpha = \frac{I_r}{(\Delta x)^3} \tag{3}$$

which compares the integrated intensity on the Raman image of a single droplet to the third power of its apparent

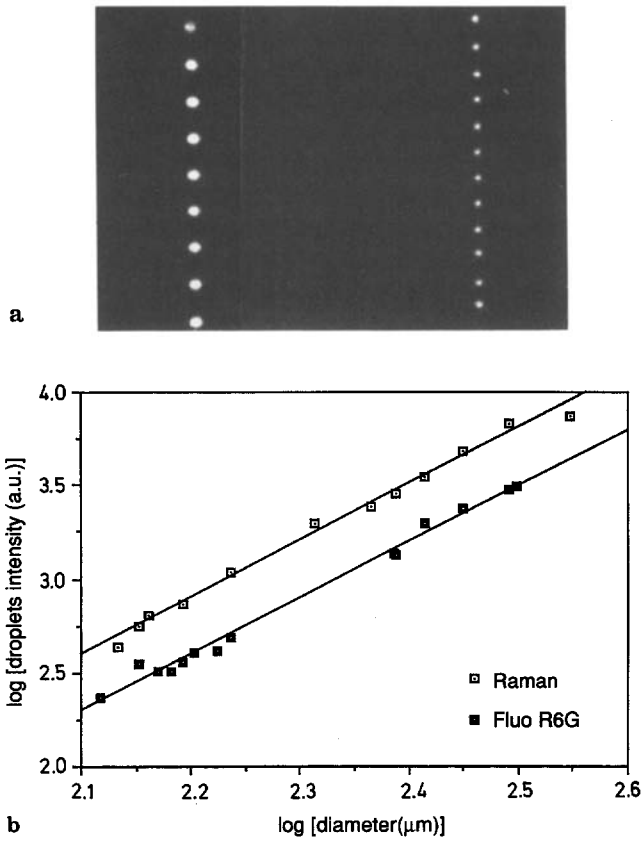

Fig. 4a, b. Calibration of the imaging system in a stream of monosized droplets. **a** Examples of Raman scattering (left) and dye fluorescence (right) images of the droplets inside the laser sheet ($e = 1$ mm in that particular case); **b** Check for linearity of integrated intensity upon droplet volume

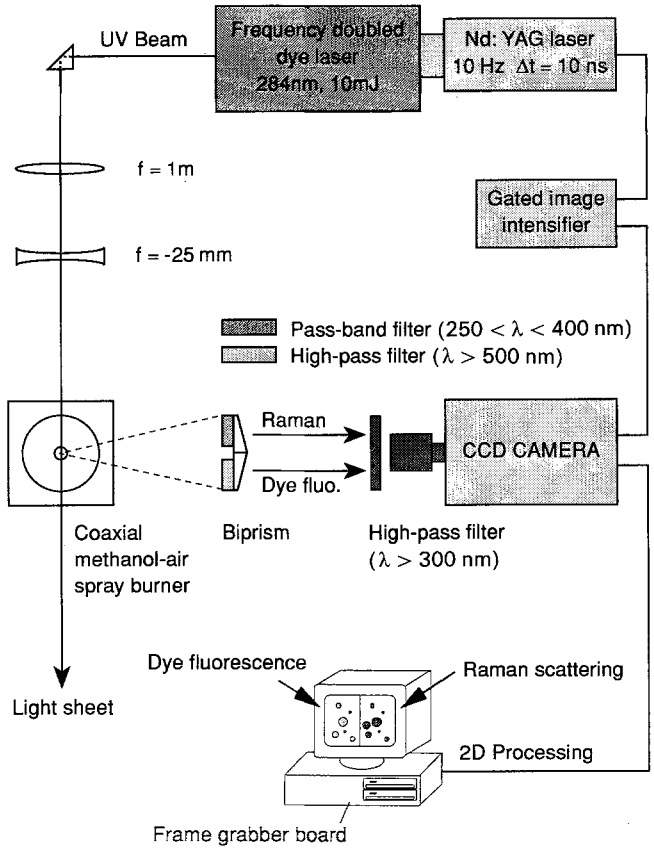

Fig. 5. Apparatus

diameter estimated on that Raman image. When a spherical droplet is completely excited by the laser field, α attains a constant value which can be determined from calibrations. Experiments in the stream of monosized droplets have confirmed that α drops from its constant level, α_0, as soon as the droplets are not completely immersed in the laser sheet. Actually, the field of application of this criterion (i.e. $\alpha = \alpha_0$) is wider as, in addition, α decreases when detector saturation occurs and it may be found higher or lower than expected when the probed droplets are not spherical.

In the spray, the pdf of α can be use to determine the normal value α_0 and the range of ratio α out of which the data must be rejected as they correspond to droplets not completely inside the laser sheet or saturated or too aspherical.

5 Apparatus and image processing (Fig. 5)

The laser measurements of fuel vaporization have been performed in the near development field of a burning spray the initial zone of which is pictured in Fig. 1. The spray is produced by a coaxial air-blast injector in which the liquid jet issues at low velocity (0.35 ms^{-1}) from a central tube and is atomized by a parallel air flow issuing at 110 ms^{-1} from an annular duct. The central tube (2 mm diameter) is fed with methanol weakly doped with rhodamin 6G ($C_0 \approx 0.02$ ppm). This injector is located at the bottom of a water-cooled chamber (8 × 8 cm) equipped with large quartz windows. Details have been described in a paper by Goix et al. (1992) which reports on phase-Doppler and OH fluorescence measurements.

The pulsed radiation ($\lambda_0 = 284$ nm, $\Delta t = 10$ ns, $\varepsilon = 10$ mJ, $f = 10$ Hz) provided by the second harmonic of a dye laser pumped by a YAG laser is focused into a vertical light sheet (20 mm height, 300 μm thick) passing through the axis of the spray. The polarization of the laser is perpendicular to the light sheet to minimize elastic scattering in the direction of fluorescence and Raman collection. The laser induced emissions are imaged at 90° onto a gated intensified *Charge-Coupled-Device* camera (Proxitronix, $\Delta t_{gate} = 50$ ns) with a 105 mm – F/4.5 objective lens equipped with a high-pass filter ($\lambda > 300$ nm) that rejects the remaining laser radiation. With the camera located 300 mm from the laser sheet, the magnification is about 0.5.

A biprism equipped with the two filters ($300 < \lambda < 390$ nm for Raman scattering and $\lambda > 480$ nm for dye fluorescence) described in Fig. 2 and 5 is interposed before the camera to split the emitted radiations into two parallel images onto the CCD. One image provides the Raman scattering intensity while the other provides the simultaneous fluorescence intensity over the same field of view (13 mm × 20 mm). The video signal is digitized by a frame grabber board (Matrox MVP-AT, 512 × 512, 8 bits) connected to a PC. Real time processing (4 Hz) is performed in two selected windows that correspond to the same imaged field of view (5 mm × 2 mm) and typical results are shown in Fig. 6a. This processing integrates the signal levels over the height of each window and the pair of radial profiles that are obtained at each laser shot are transferred to the PC where they are stored and post-processed (see Fig. 6b). Calibrations of the whole system

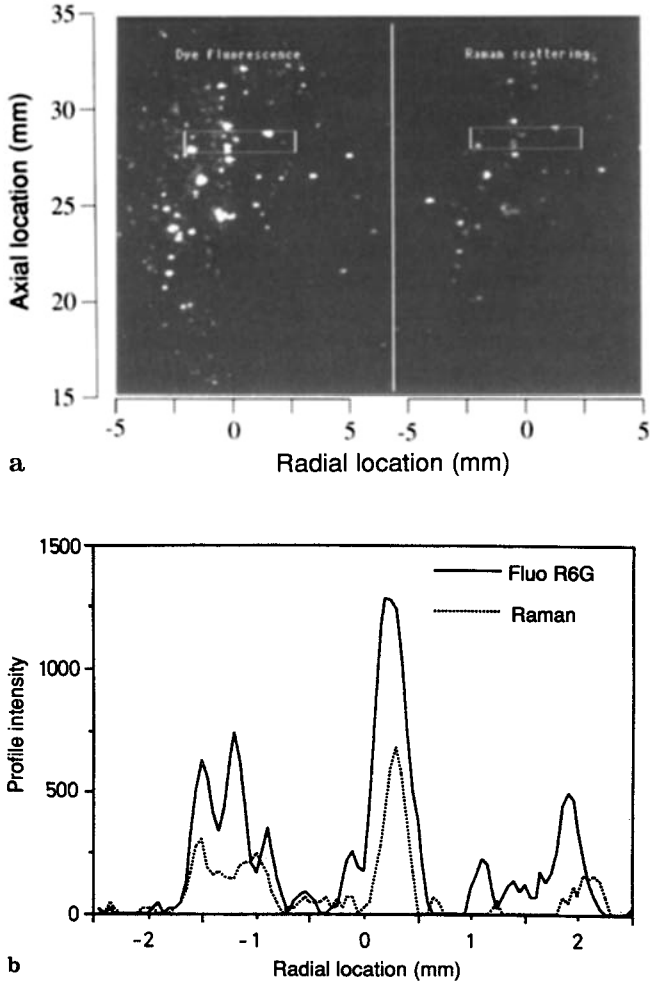

Fig. 6a, b. Processing of the two parallel images. **a** Example of two parallel images (dye fluorescence on the left, Raman scattering on the right) simultaneously induced by a single laser shot in the burning spray **b** Pair of radial profiles in the two selected windows shown in Fig. 6a

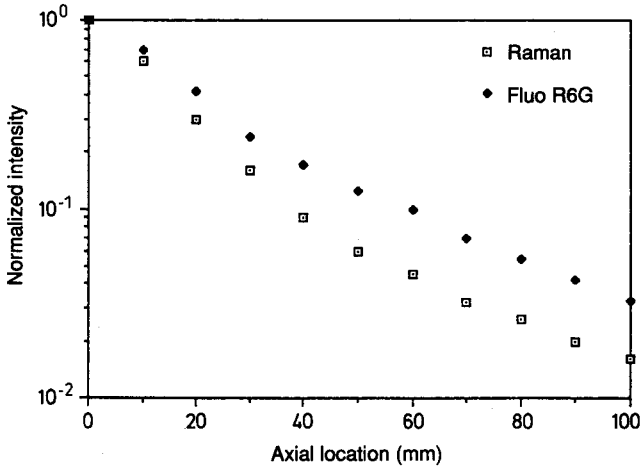

Fig. 7. Centerline decays of the integrated Raman and fluorescence signal levels (average over 200 shots)

are performed under reference conditions (in the liquid core of the cold jet and in the stream of monosized droplets) to equalize the simultaneous signal intensities and to optimize the dynamic range of the intensified CCD.

6 Experimental results and discussion

6.1 Mass flux of vaporization along the spray axis

The radial profiles of fluorescence and Raman signal intensities in the observed window have been integrated and averaged over 200 laser shots. Figure 7 shows the center line decays of these averaged values in the burning spray as a function of the height above the injector.

Basically, the fluorescence decay is only due to the spray dispersion as the mass weighted number of droplets passing through the window decreases with elevation, while the decay of Raman scattering is due to both dispersion and vaporization of the spray. Thus, the relative difference, $1-\bar{I}_r/\bar{I}_f$, between fluorescence and Raman intensities, which is plotted in Fig. 8 as a function of the probing height, measures the mass fraction $\phi(h)$ of methanol that has been vaporized in the stream tube up to the probed volume independently of spray dispersion. However, the droplets which have completely vaporized before their trajectory crosses the probing window are not accounted for since the fluorescence yield vanishes as $(d/d_0)^3$ approaches zero (see Fig. 3). Let's $\bar{I}'_f = \bar{I}_f/\beta$ be the ideal fluorescence intensity as if the fluorescence yield were constant including when $d/d_0 = 0$ (i.e. to the solid phase). Then, the actual mass fraction ϕ' of methanol that has been cumulatively vaporized over the spray axis up to h can be extrapolated by using:

$$\phi'(h) = 1 - \beta(h) + \beta(h)\phi(h) \qquad (4)$$

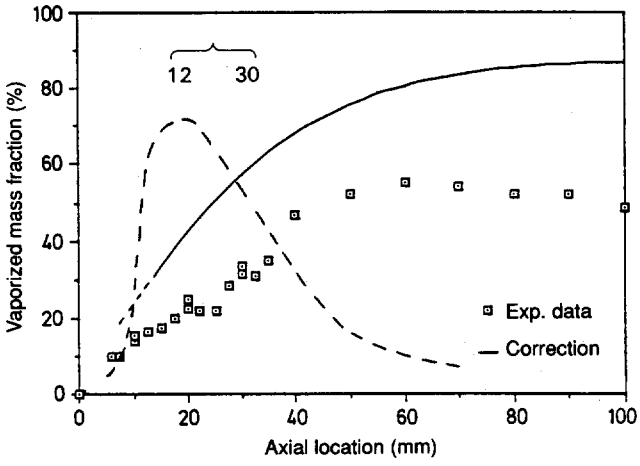

Fig. 8. Mass fraction of vaporized fuel along axis of burning spray. □ □ □: relative difference between fluorescence and Raman intensities; (——): cumulative mass fraction of vaporized fuel; this corrected curve accounts for the contribution of the droplets that have completely vaporized before the probing event; (– – –): reduced rate of vaporization per length unit along the spray axis. The brace marks the zone of flame stabilization

The procedure for estimating the correction factor $1/\beta(h)$ is described in 6.3. The uncertainty on β is about ± 0.1 in the worst case where $\beta \approx 0.8$ ($h \approx 25$ mm). As $\Delta\phi/\phi \approx 15\%$, the uncertainty on ϕ' is ± 0.1. The full line in Fig. 8 shows how the corrected mass fraction of vaporized fuel continues to increase on the axis toward complete vaporization.

The derivative of the cumulative mass fraction of vaporized fuel versus h provides a reduced rate of vaporization per length unit. The dashed curve in Fig. 8 shows that most of the fuel vapor production on the spray axis takes place between 12 and 30 mm above the injector which is the range of lift-off heights where the flame is stabilized (Goix et al. 1992).

6.2 Surface reduction of the droplets, evaporation constant

In a quiescent homogeneous environment the diameter of a spherical droplet decays (Spalding 1953) according to $d^2 = d_0^2 - kt$ where k is the evaporation constant. The simultaneous fluorescence and Raman signal in the observed window have been analyzed in term of area under the corresponding peaks, I_f and I_r respectively, on the radial profiles. As these area are proportional to d_0^3 and d^3 respectively (in so far as the detected peaks correspond with single spherical droplets completely inside the laser sheet), the value of $A = \alpha_0^{-2/3}(I_f^{2/3} - I_r^{2/3})$ for each pair of peaks is a direct measure of $\int k dt$ where the vaporization constant is integrated over the time of flight of the spherical droplet through the burning spray environment up to the laser probing event. For aspherical droplets, even-

though the theorical linear decay of d^2 is extended to a linear decay of the area of the droplet surface, the value of α (which is above or below α_0, depending on orientation of the drop) cannot be determined. A validation procedure is required to select the peaks for which $\int k dt = A$ (i.e. the peaks corresponding with spherical droplets).

Along with the area, the Raman peakwidth is stored, and for each station of the window on the spray axis, the pdf of $\alpha = I_r/(\Delta x)^3$ is used to reject the marginal data ($|\Delta\alpha/\alpha_0| > 30\%$) associated with droplets that are not completely inside the laser sheet or too aspherical or with overlapped projections onto the radial profiles. Examples of pdfs of α are shown in Fig. 9: in the near field of the spray development the pdf broadness reduces the number of validated data. For larger distances ($h > 25$ mm) the validation rate improves, but the number of probed droplets is reduced by the dispersion of the spray.

For each station on the spray axis, the scatter plot of $1-(I_r/I_f)^{2/3}$ versus $\alpha_0^{2/3} I_f^{-2/3}$ has been used to estimate the value of $A = \int k dt$ from the slope of the regression straight line along with the coefficient of correlation with respect to that linear law. This correlation has appeared to be highly improved by the validation procedure. The axial profile of $A(h) = \int_0^h k(h)/v(h)\, dh$ which is plotted in Fig. 10 together with the correlation coefficient, provides cumulative information on the dynamic evaporation rate undergone by the droplets. Although the temperature is low in the early stages, both the convection induced enhancement of k and the long residence time of the inertial droplets in that environment lead to noticeable levels of A as soon as they can be measured ($h \approx 15$ mm). Between 15 and 20 mm above the injector A is nearly constant with a downward trend that cannot be ascertained, as both the validation rate and the correlation coefficient are low. The conditions for the d^2 law to apply are far from being fulfilled in this region of high fluctuations where the turbulent boundary layers reach the jet axis. Therefore, this tendency could be an effect of secondary break-up of the droplets in this zone as the measurements of A is known to be biased downward if such break-up occurs. Beyond 20 mm above the injector $A(h)$ increases regularly along with the correlation to the d^2 law. As phase-Doppler measurements (Goix et al. 1992) show that the velocity of the large droplets ($d > 50$ μm) is nearly constant in this region, the regular increase of A can be attributed to the higher value of k in the combustion zone. The derived evaporation constant, $k \approx 2.10^{-6}$ mm$^2 \cdot$s^{-1}, is somewhat higher than the value to be expected for a quiescent non-reactive environment at the flame temperature (Chigier and McCreath 1974).

6.3 Droplet consumption

As the fluorescence yield drops sharply when d/d_0 approaches zero, the contribution of the droplets which have

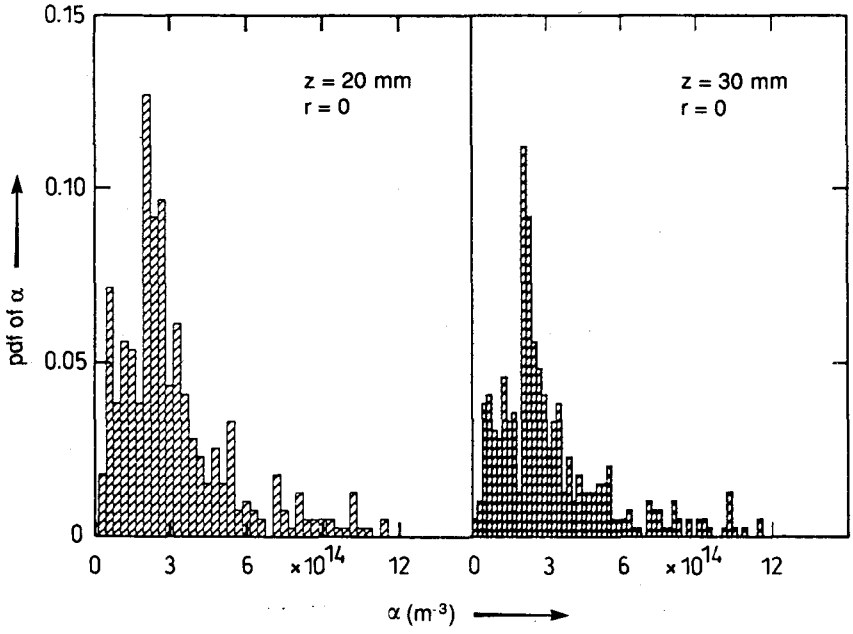

Fig. 9. Criterion for rejecting the droplets not completely inside the laser field or too aspherical. α compares the integrated intensity on the Raman image of a single droplet to the third power of its apparent diameter.

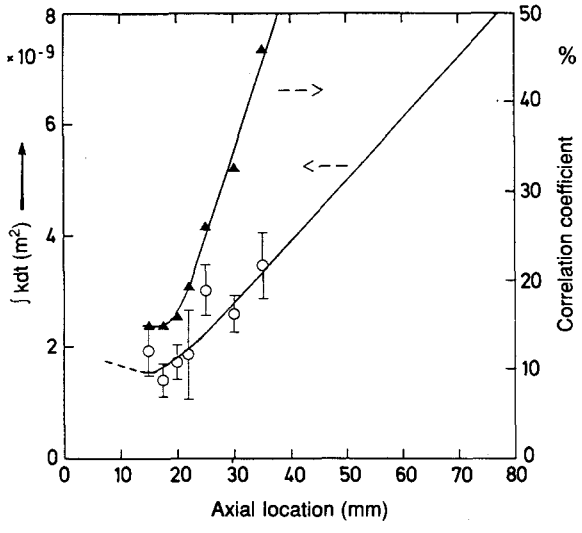

Fig. 10. Cumulative evolution of vaporization constant along axis of the burning spray. The coefficient of correlation with respect to the d^2 law is although provided

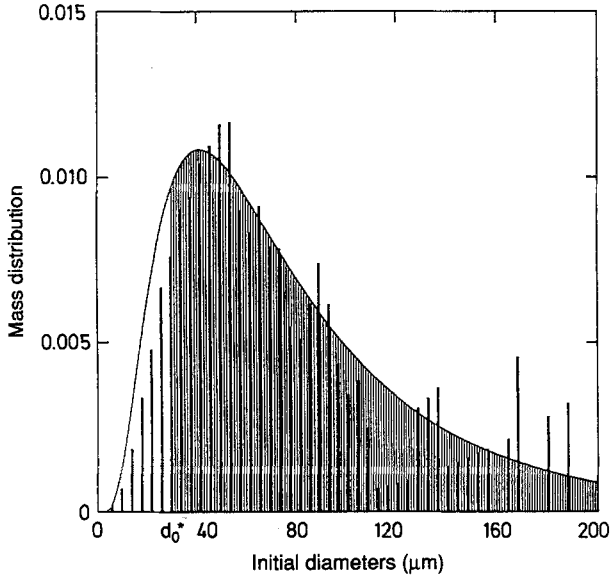

Fig. 11. Distribution of $d_0^3 p(d_0)$. Full line is the log-normal function fitted to the distribution (vertical bars) derived from the phase-Doppler measurements. Dashed area from the cut-off value, d_0^*, is the global fluorescence intensity as consumpted droplets are no longer accounted for

completely vaporized is not accounted for by the measurements that are performed in term of mass budget in a probed volume (Sect. 6.1). The droplet size distribution from phase-Doppler measurements (5 μm–200 μm) in the early stage of the spray development (Goix et al. 1992) has been fitted to the log-normal distribution function (Lefebvre 1989) so as to reform the tail ($d_0 > 100$ μm) over which precise experimental data were lacking. This size distribution is then weighted by d_0^3 so that area, $\int_0^\infty d_0^3 p(d_0) dd_0$, shown in Fig. 11 represents the global fluorescence intensity I_f° at the injector exit. As evaporation takes place, the droplets with initial diameter d_0 smaller than d_0^*—with $(d_0^*)^2 \approx \int k dt = \int_0^h (k/v) dh$—are no longer accounted for in the integration and, accordingly the global fluorescence intensity I_f is reduced ($I_f/I_f' = \beta$) as is the dashed area in Fig. 11. The normalized growth of $1 - \beta(d_0^*) \equiv \int_0^{d_0^*} d_0^3 p(d_0) dd_0$ is plotted in Fig. 12a. Using the

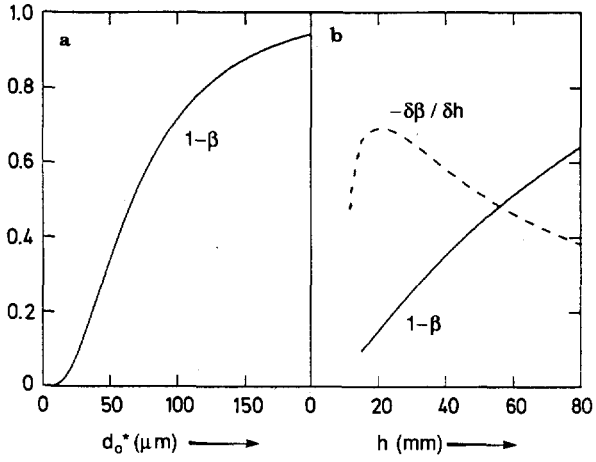

Fig. 12. **a** Contribution (to the ideal fluorescence signal) of consumpted droplets (with $d_0 < d_0^*$) which are not accounted for; **b** Growth of the probability, $1-\beta$, that the droplets have completely vaporized before reaching elevation h on the axis. The dashed curve represents the density of probability that consumption of the droplets occurs at elevation h

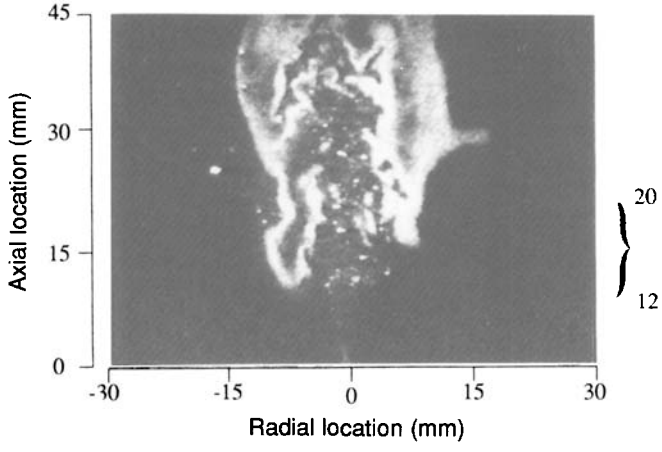

Fig. 13. Example of single shot planar laser induced fluorescence of OH radical in the burning spray. Discrete spots are only due to Raman scattering from liquid fuel as Mie scattering was rejected by high-pass filtering (Goix et al. 1992). The brace marks the range of heights where flame stabilization occurs.

experimental dependence of $\int_0^h k/v\, dh$ on h (see Sect. 6.2) the growth of $1-\beta$ can be obtained as a function of the height above the injector (Fig. 12b). The uncertainty on $\beta(h)$ is maximum ($\Delta\beta \approx \pm 0.1$) at the inflection of $\beta(d_0^*)$ which occurs at $h \approx 25$ mm ($\beta \approx 0.8$). This estimate of $\beta(h)$ has been used to correct the cumulative mass fraction of vaporized fuel (Sect. 6.1) for the bias due to full droplet consumption before probing. $1-\beta(h)$ can be interpreted as the probability—in term of mass—that the droplets have completely vaporized before reaching elevation h on the axis. Therefore $-\partial\beta/\partial h$ (the dashed curve in Fig. 12b) represents the density of probability that full consumption of the droplets occurs at elevation h. The range of height where fuel consumption is most probable fits with the zone where combustion takes place on the spray axis ($h \approx 20$ mm) as shown by planar OH fluorescence mappings (see Fig. 13).

7 Concluding remarks

A linear measurement technique based on single shot planar laser induced fluorescence and Raman scattering in liquid phase has been studied and applied in the early development of a burning spray for statistic investigation of the vaporization dynamics. Calibrations in a stream of monosized droplets have shown that over the dynamic range of the imaging system the intensity on the droplets images are proportional to the actual droplet volume, d^3, for Raman scattering and to the initial droplet volume, d_0^3, for the dye fluorescence. A test has been implemented to reject the data corresponding to droplets that are not completely inside the laser sheet or too oblong. This validation procedure has proven to be crucial when the data are analyzed in terms of size reduction of individual droplets to investigate the evaporation constant according to the d^2 law. It should be interesting to analyze the vaporization dynamics with size-classified data. Such a statistical analysis is made difficult by the low number of available samples; in the initial zone the validation rate is low; downstream on the axis the number of droplets in the observed window is reduced by spray dispersion and combustion.

In the very severe experimental conditions that are met in the early development zone of the burning spray, the technique has provided axial data on the vaporization dynamics before and over the region where combustion takes place. The contribution of the smallest droplets ($d < 50$ μm) to the vaporization rate was not directly accounted for as the finite dynamic range of the imaging system limits the investigated size range (50 μm–300 μm). In addition, the droplets that have completely vaporized before reaching the probed volume were not accounted for, but a satisfactory correction for this bias and statistical data on the rate of droplet consumption have been obtained by using the droplet size distribution from phase-Doppler measurements in the initial zone. This result underscores the usefulness of performing conjoined measurements in these complex flows.

Acknowledgements

This work was supported by PRC "combustion dans les moteurs fusées" (CNES-CNRS-SEP). The authors thank J. B. Blaisot for

his assistance, and D. Stepowski is grateful to G. Searby for discussions.

References

Bruhat, G. 1992: Fluorescence et phosphorescence. In: Cours de Physique Générale, Optique (ed Kastler A). Paris Milan Barcelone Bonn, pp 827–851

Chigier, N. A.; McCreath, C. G. 1974: Combustion of droplets in sprays. Acta Astronautica 1:687–710

Goix, P. J.; Edwards, C. F.; Cessou, A.; Dunsky, C. M.; Stepowski, D. 1992: Structure of a methanol/air coaxial reacting spray near the stabilization region. Combust and flame, under press

Herzberg, G. 1945: Infrared and Raman spectra of polyatomic molecules. In: Molecular spectra and molecular structure. Van Nostrand Company, Princeton, NY pp 323–336

Johnston, S. C. 1981: An experimental investigation into the application of spontaneous Raman scattering to spray measurements in an engine. ASME fluid mechanics of combustion systems symposium, Boulder, Colorado, June 22–24

Lefebvre, A. H. 1989: Drop size distribution of sprays. In: Atomization and spray. Hemisphere Publishing Corporation, New York Washington Philadelphia London, pp 79–103

Melton, L. A.; Verdieck, J. F. 1985: Vapor/liquid visualization for fuel spray. Combust. Sci and Tech 42:217–222

Miles, R. B.; Lempert, W. R.; Forkey, J. 1990: Imaging turbulence in high-speed air by filtered Rayleigh scattering. 12th Symposium in Turbulence. University of Missouri-Rolla, September 24–26

Serpenguzel, A.; Swindal, J. C.; Chang, R. K.; Acker, W. P. 1992: Two-dimensional imaging of spray with fluorescence lasing and stimulated Raman scattering. Appl. Optics 31:3543–3551

Spalding, D. B. 1953: The combustion of liquid fuel. 4th Symposium (international) on Combustion 847–864